Available online at www.sciencedirect.com
ScienceDirect
Journal of Solid State Chemistry 179 (2006) 2751–2760
JOURNAL OF SOLID STATE CHEMISTRY
www.elsevier.com/locate/jssc

Mg_8Rh_4B — A new type of boron stabilized Ti_2Ni structure

A.M. Alekseeva[a,b,*], A.M. Abakumov[a,b,c], A. Leithe-Jasper[a], W. Schnelle[a], Yu. Prots[a], P.S. Chizhov[a,b], G. Van Tendeloo[c], E.V. Antipov[b], Yu. Grin[a]

[a]*Max-Planck-Institut für Chemische Physik fester Stoffe, Nöthnitzer Straße 40, 01187 Dresden, Germany*
[b]*Department of Chemistry, Moscow State University, Moscow 119992, Russia*
[c]*EMAT, University of Antwerp, Antwerp B-2020, Belgium*

Received 17 October 2005; received in revised form 17 November 2005; accepted 18 November 2005
Available online 4 January 2006

Abstract

The new magnesium rhodium boron compound Mg_8Rh_4B has been synthesized by reaction of the metal powders with crystalline or amorphous boron or the RhB precursor. The crystal structure of Mg_8Rh_4B was solved using single-crystal X-ray diffraction data (space group $Fd\bar{3}m$, $a = 12.1711(4)$ Å, $Z = 8$, 174 reflections, $R_F = 0.016$). The crystal structure can be described as a filled Ti_2Ni type where the interstitial sites 8*b* ($\frac{1}{2}, \frac{1}{2}, \frac{1}{2}$), located at the center of two nested Mg_4Rh_4 tetrahedra, are occupied by boron atoms. Taking into account the absence of the Ti_2Ni-type phase in the binary Mg–Rh system, the boron atoms can be considered as stabilizing this structural motif. From the bonding analysis with the electron localization function the crystal structure is described as covalently bonded $[Rh_4B]^{3-}$ anions, embedded in a cationic magnesium matrix.

Keywords: Mg_8Rh_4B; Synthesis; Crystal structure; Stabilization of the Ti_2Ni type of structure

1. Introduction

The Ti_2Ni type of crystal structure is frequently found for binary intermetallic compounds of transition metals with A_2M composition (so-called η phases). In rare cases, the 16*d* position filled by the *A* component in Ti_2Ni type is occupied by the *M* component and the total composition changes to *AM*. This derivative from the Ti_2Ni structure type is called NiCd [1]. The main feature of the Ti_2Ni structure type is the ability to incorporate non-metal elements like H, C, N, O [2,3]. For this reason, the η phases have attracted recently significant attention as promising hydrogen storage materials [4–10].

Some transition elements can form "pure" binary η phases without interstitial elements, e.g. Hf_2Co, Hf_2Mn and Hf_2Fe [6,7,11–13], other phases exist only in the presence of interstitial elements, e.g. Hf_2PdO_x, Hf_2NiO_x, Ti_2FeO_x [11,13,14].

The most-widely known groups of Ti_2Ni-type compounds are subcarbides and suboxides of transition metals. Neutron powder diffraction structure investigation of some of η-carbides and η-oxides [10,14–16], and structure determinations from single-crystal X-ray diffraction data, performed for Zr_4Ni_2O, Nb_6Ni_6O, $Zr_6Ni_4Ti_2O_{0.6}$ and $Nb_6Ni_4Ta_2O_2$ [17], show that oxygen or carbon atoms partially occupy the octahedrally coordinated interstitial sites. The large number of Ti_2Ni-type transition metal subcarbides allows in discussing the tendency of formation of metal-carbon octahedra for different transition metals [18,19].

The $Mg_2Rh(H,D)_{1.1}$ compound is the first representative of the Ti_2Ni structure type, stabilized by hydrogen incorporation [20]. Neutron diffraction data refinement reveals that the hydrogen and deuterium atoms mainly occupy the tetrahedral interstitial voids, whereas the octahedral voids exhibit much smaller partial occupation.

Two boron containing Ti_2Ni-type compounds, $Nb_2NiB_{0.16}$ [21] and Re_3Al_2B [22], were previously

*Corresponding author. Max-Planck-Institut für Chemische Physik fester Stoffe, Nöthnitzer Straße 40, 01187 Dresden, Germany.
Fax: +0049 0 351 4646 4002.
E-mail address: alekseev@cpfs.mpg.de (A.M. Alekseeva).

0022-4596/$ - see front matter © 2005 Elsevier Inc. All rights reserved.
doi:10.1016/j.jssc.2005.11.029

reported. For both phases the boron incorporation can be considered as stabilizing the Ti_2Ni-type structure because of the absence of binary η phases in the Nb–Ni and Re–Al systems [21,22]. The Ti_2Ni type of the crystal structure for $Nb_2NiB_{0.16}$ and Re_3Al_2B was established by X-ray powder diffraction. A model for the crystal structure of $Nb_2NiB_{0.16}$ was proposed on the basis of the similarity of the X-ray powder data with the η phase Nb_2NiE_x, E = C, N, O [23]. Boron atoms are suggested to occupy the octahedrally coordinated interstitial sites. The Re_3Al_2B phase was supposed to be isostructural with Mn_3Ni_2Si [24], the crystal structure of which is characterized as a Ti_2Ni-type atom arrangement, where the position 16*d* is occupied by silicon atoms. The boron atoms in Re_3Al_2B are assumed to be located at the 16*d* position with octahedral coordination. However, for both compounds, $Nb_2NiB_{0.16}$ and Re_3Al_2B, a precise determination of the boron atom positions was not performed.

In this contribution we describe preparation and chemical bonding of the new ternary magnesium rhodium boron compound Mg_8Rh_4B, a first representative of the Ti_2Ni derivative with boron atoms occupying tetrahedral voids.

2. Experimental

Mg_8Rh_4B samples were prepared starting from powders of magnesium (Alfa Aesar, 99.8%) and rhodium (Chempur, 99.9%), amorphous (Alfa Aesar, 99.99%) or crystalline boron (Alfa Aesar, 99.999%). The oxygen content in the initial materials was determined by the carrier gas hot extraction method (combined infrared and heat-conduction detector TC 436 DR/5, LECO, USA). The oxygen content was found to be lower than the detection limit (0.038 wt%) in rhodium and crystalline boron powder, 0.05–0.2 wt% in the magnesium powder and ~4 wt% in amorphous boron.

The sample preparation was carried out in several steps. First, the crystalline boron (B_{cr}) was converted into the RhB precursor. For this purpose a fraction of B_{cr} with a particle size $\leqslant$20 μm was arc-melted with the stoichiometric amount of Rh in an argon atmosphere. A formation of the single-phase RhB was confirmed by X-ray powder diffraction. The obtained rhodium monoboride was ground in a tungsten carbide mortar and intimately mixed with appropriate amounts of magnesium and rhodium powders in an agate mortar, pressed into pellets and sealed into tantalum containers (diameter 8 mm, length 25 mm). All operations were performed in a glove box under argon atmosphere (content of O_2 and $H_2O \leqslant 0.1$ ppm). The tantalum containers were sealed into evacuated silica ampoules and annealed at 850–1000 °C for 3–7 days with one intermediate re-grinding in argon atmosphere. The ampoules were finally cooled in the furnace to 40 °C.

Phase identification and lattice parameter determination were performed using room-temperature X-ray powder diffraction data (image plate Guinier camera Huber G670, $CuK_{\alpha 1}$ radiation, $\lambda = 1.540598$ Å) with LaB_6 as internal standard ($a = 4.15690(5)$ Å). The crystal structure was determined using single-crystal X-ray diffraction data collected with a Rigaku AFC 7 (Mercury CCD) diffraction system. Crystallographic information and details of the data collection are given in Table 1. All crystallographic calculations were performed with the WinCSD program package [25].

Table 1
Data collection and crystallographic information for Mg_8Rh_4B

Composition	Mg_8Rh_4B
Crystal shape	Irregular
Crystal size/mm^3	$0.025 \times 0.045 \times 0.09$
Crystal system	Cubic
Space group	$Fd\bar{3}m$
a/Å	12.1711(4)[a]
V/Å^3	1803.0(2)[a]
Z	8
Radiation, λ/Å	Mo$K\alpha$, 0.71073
Max. $\sin\theta/\lambda$	0.749
Calculated density/g cm^{-3}	4.547(1)
Absorption coefficient/cm^{-1}	74.48
Measured reflections	3417
Independent reflections	176
R_{eq}	0.034
Reflections used for refinement	174
Number of parameters refined	12
Extinction coefficient[b]	0.00052(3)
$R(F)$, $R(F^2)$ for $F(hkl) \geqslant 4\sigma(F)$	0.016, 0.020
Largest diff. peak (e$^-$ Å^{-3})	0.5

[a]From X-ray powder diffraction data.
[b]Extinction coefficient was refined as: $k[1 + 0.001Fc^2\lambda^3/\sin(2\theta)]^{-1/4}$, k is overall scale factor [58].

Differential thermal analysis (DTA) was carried out in the range from room temperature to 1300 °C (STA 409, Netzsch, thermocouple type S, 30–60 mg per sample) in niobium containers sealed in argon atmosphere with a heating–cooling rate of 10 K/min.

Metallographic investigation was performed on polished samples with a Zeiss Axiotec 100 optical microscope equipped with polarizer and analyzer. The whole setup, including the polishing system, is located in an argon-filled glove box in order to protect the material against reaction with air and moisture [26]. The chemical composition was analyzed with a Philips XL30 scanning electron microscope equipped with an Edax Phoenix EDX detector. EDXS measurements were performed with Mg–*K* and Rh–*L* lines at three points for each phase.

Specimens for transmission electron microscopy were prepared by crushing the polycrystalline sample Mg_8Rh_4B in ethanol and placing the fragments on a carbon grid. Electron diffraction (ED) patterns were obtained using a Philips CM20 electron microscope.

Magnetisation was measured in a SQUID magnetometer (MPMS-XL7, Quantum Design) in fields ranging from 20 Oe to 70 kOe and temperatures between 1.8 and 400 K. The electrical resistance was determined by a conventional

four-contact DC measurement between 3.8 and 320 K. Thin Pt wires were attached to the sample using silver-filled epoxy glue. Due to the geometry of the samples an inaccuracy of $\pm 50\%$ is estimated for the absolute resistivity values.

Electronic structure calculation and bonding analysis were carried out using the TB-LMTO-ASA program package [27]. The Barth–Hedin exchange potential [28] was employed for the LDA calculations. The computation was made for $8 \times 8 \times 8$ k-points in an irreducible wedge of the Brillouin zone. The tetrahedron method was implemented for the integration over the Brillouin zone with nine inequivalent tetrahedra. The radial scalar-relativistic Dirac equation was solved to get the partial waves. Although the calculation within the atomic sphere approximation (ASA) includes corrections for the neglect of interstitial regions and partial waves of higher order [29], an addition of empty spheres for both compounds was necessary. The following radii of the atomic and empty spheres were applied for the calculations for the Mg_8Rh_4B compound: $r(Mg1) = 1.752$ Å, $r(Mg2) = 1.758$ Å, $r(Rh) = 1.278$ Å, $r(B) = 1.045$ Å, $r(E) = 1.055$ Å. A basis set containing Mg($3s, 3p$), Rh($5s, 5p, 4d$) and B($2s, 2p$) orbitals was employed for a self-consistent calculation with Mg($3d$), Rh($4f$) and B($3d$) functions being downfolded.

The electron localization function (ELF, η) was evaluated according to [30] with an ELF module implemented within the TB-LMTO-ASA program package [27]. The topology of ELF was analyzed using the program Basin [31] with consequent integration of the electron density in basins, which are bound by zero-flux surfaces in gradient field. This procedure, similar to the one proposed by Bader for the electron density [32], allows to assign an electron count for each basin, revealing the basic information about the chemical bonding.

3. Results and discussion

3.1. Synthesis and composition characterization

The Mg_8Rh_4B phase was obtained first by a direct reaction of magnesium and rhodium powders and amorphous boron in tantalum containers sealed in argon atmosphere at 1000 °C for 5 days. However, the prepared samples contained about 5% of MgRh and 2–3% MgO impurities. Amorphous boron was found to act as the source of oxygen. Therefore crystalline boron was chosen as much more suitable for preparing single-phase samples in spite of its low reactivity. The difficulty of directly reacting the initial materials is reflected by the difference in their melting points [33]: Mg—650 °C, Rh—1960 °C, and B_{cr}—2074 °C. In order to overcome this complication, RhB (melting temperature 1140 °C) was used as a precursor for synthesis.

The best Mg_8Rh_4B sample was prepared by heat treatment of a mixture of RhB, Mg and Rh at 850 °C for 7 days followed by quenching in water. The obtained sample contained the Mg_8Rh_4B phase with small amounts of MgO (~1%) and an additional phase (~2%). The X-ray powder diffraction pattern (Fig. 1) was indexed with a face-centered cubic lattice and an unit cell parameter $a = 12.1711(4)$ Å. The phase composition of the prepared sample was confirmed by metallographic analysis and EDXS investigation. The main phase with a Mg/Rh ratio of 1.99(3), which corresponds to Mg_8Rh_4B, was found together with a small amount of the additional phase (cf. XRD data above), because of very small size of the particles of this, the composition could not be distinguished. According to the results of differential thermal analysis, Mg_8Rh_4B decomposes at 1080 °C. The X-ray diffraction pattern of the sample cooled down after melting showed the presence of Mg_8Rh_4B together with Mg_5Rh_2 and MgRh, indicating an incongruent formation.

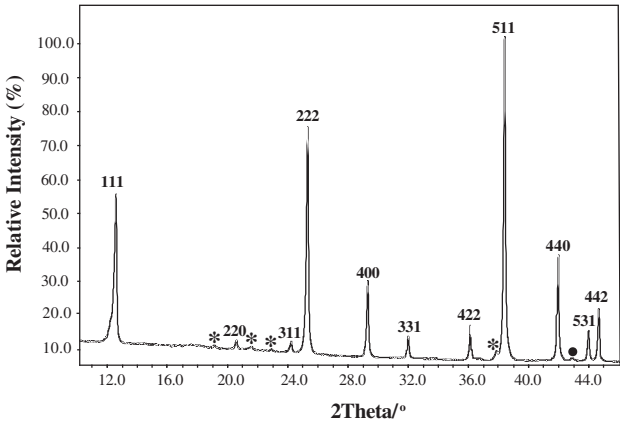

Fig. 1. X-ray powder diffraction pattern of Mg_8Rh_4B. Reflections of the admixture phases are marked as stars (additional phase) and filled circles (MgO).

Single crystals of Mg_8Rh_4B suitable for X-ray analysis were prepared by annealing the Mg_8Rh_4B sample at 1100 °C in a sealed tantalum container for 30 min and cooling down to 400 °C within 24 h. EDXS measurements, performed on three different single crystals, resulted in a metal ratio Mg/Rh = 1.99(14), which agrees well with the composition found in the bulk sample and with the results of the crystal structure determination.

3.2. Structure determination of Mg_8Rh_4B

The reciprocal lattice of Mg_8Rh_4B was investigated by electron diffraction. The electron diffraction patterns taken along the most relevant zone axes are shown in Fig. 2. All patterns can be completely indexed with a face-centered cubic lattice and a unit cell parameter as determined from X-ray powder diffraction. The following reflection conditions were observed: $h\,k\,l$ with $h + k = 2n$, $k + l = 2n$, $l + h = 2n$; $0\,k\,l$ with $k = 2n$, $l = 2n$, $k + l = 4n$; $h\,h\,l$ with $h + l = 2n$; $h\,0\,0$ with $h = 4n$. The extinctions are compatible with the space groups $Fd\bar{3}m$ and $Fd\bar{3}$. The forbidden reflections $0\,0\,l$: $l \neq 4n$ (e.g. 002), present on the [110]*

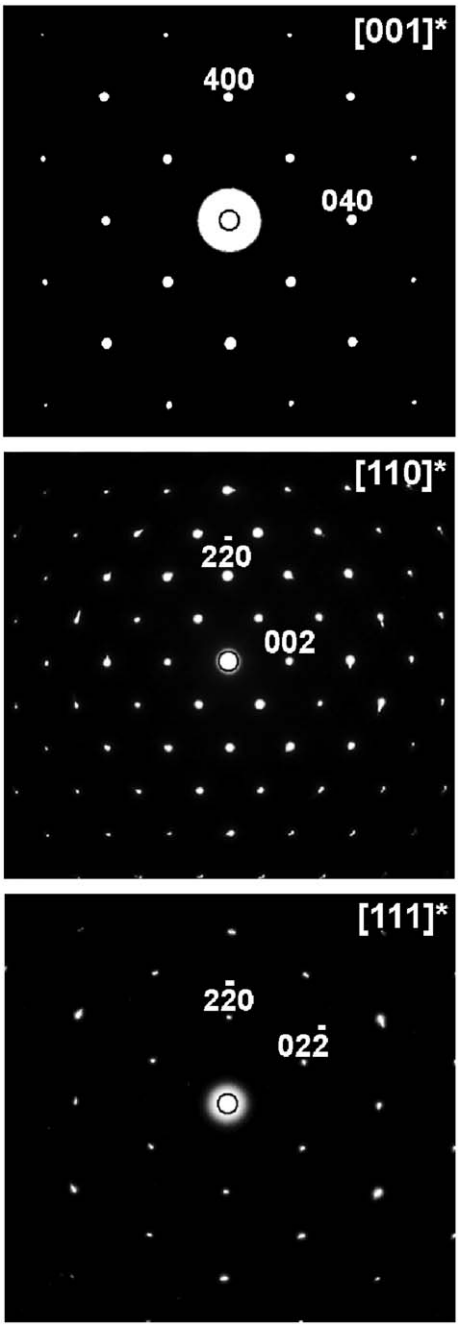

Fig. 2. Electron diffraction patterns of Mg_8Rh_4B along [001]*, [110]* and [111]*.

pattern, are caused by multiple diffraction, as was confirmed by the absence of these reflections in the [001]* pattern.

The crystal structure was determined using single-crystal X-ray diffraction intensities. Crystallographic data and details of the data collection are listed in Table 1. The space group $Fd\bar{3}m$ was chosen from intensity statistics for the further structure solution and refinement. The initial atomic coordinates of Rh and Mg atoms were determined using direct methods. Boron atoms were located in the difference Fourier map. The refinement of the crystal structure was performed with an anisotropic description for the atomic displacement parameters (ADP) of Mg and Rh atoms, whereas the displacement for the boron position was refined isotropically. The difference Fourier map after refinement did not show any significant residual electron density peaks, the value of the maximum difference electron density peak was found to be $0.5\,e^-\,Å^{-3}$. Final structural parameters are listed in Table 2 and selected interatomic distances are presented in Table 3.

3.3. The crystal structure of Mg_8Rh_4B

The crystal structure of Mg_8Rh_4B belongs to the filled Ti_2Ni structure type. From a geometrical point of view the structure can be described as two interpenetrating frameworks formed by octahedra and tetrahedra. The octahedral framework is constituted by Mg1 atoms at the 48*f* position and contains two different types of $(Mg1)_6$ octahedra. The $(Mg1)_6$-I octahedra around the 8*a* (0, 0, 0) position are regular with an edge length of $d(Mg1-Mg1) = 3.431(2)$ Å. All $(Mg1)_6$-I octahedra are isolated from each other (Fig. 3a). The $(Mg1)_6$-II octahedra with the centers at the 16*c* $(\frac{1}{8},\frac{1}{8},\frac{1}{8})$ positions are strongly distorted and have edges of two different lengths: 3.1649(5) Å and 3.431(2) Å. In the ideal Ti_2Ni structural motif the coordinates of the *A*1 metal atom, occupying the 48*f* position, are $(0.1875, 0, 0)$ and the coordinates of the *A*2 atom, occupying the 16*d* position, are $(\frac{5}{8},\frac{5}{8},\frac{5}{8})$ [17]). The octahedra of type II are regular. Shifting the *A*1 atom from its ideal position leads to a distortion of the octahedra of type II. The $(Mg1)_6$-II octahedra share all vertices with each other (Fig. 3b) and have four common lateral faces with the $(Mg1)_6$-I octahedra (Fig. 3c).

The tetrahedral framework is formed by the $Rh_4(Mg2)_4$ *stellae quadrangulae* [34] (Fig. 3d), which are the coordination polyhedron of the boron atoms (Fig. 4a). The Rh_4 tetrahedra with an edge length of 3.2779(4) Å are centered by the *B* atoms ($d(Rh-B) = 2.0073(3)$ Å). Each tetrahedral face is capped by the Mg2 atom, which forms the second coordination sphere around the boron atoms—the regular tetrahedra ($d(Mg2-Mg2) = 4.3027(1)$ Å, $d(Mg2-B) = 2.6350(4)$ Å, $d(Mg2-Rh) = 2.7287(3)$ Å). The interpenetration of the octahedral and tetrahedral frameworks is shown in Fig. 3e.

The Mg1 atoms are situated inside the polyhedron $Rh_4(Mg1)_8(Mg2)_2$, which can be described as a bicaped pentagonal prism with two additional atoms in front the $(Mg1)_2(Mg2)_2$ side faces (Fig. 4b). The coordination environment of the Mg2 atoms is composed of 12 metal atoms situated at the corners of an icosahedron and two boron atoms, placed in front of the triangular Rh_3 faces (Fig. 4c). Twelve metal atoms surrounding the Rh atom are situated at the vertices of a distorted icosahedron with one additional vertex occupied by a boron atom (Fig. 4d).

The new ternary compound Mg_8Rh_4B is considered as a Ti_2Ni structural motif stabilized by incorporation of boron atoms. In the crystal structure of $Nb_2NiB_{0.16}$ [21] boron

Table 2
Atomic coordinates and displacement parameters for Mg_8Rh_4B

Atom	Site	x/a	y/b	z/c	$B_{eq/iso}$/Å^{2} [a]	
Mg1	48*f*	0.1993(1)	0	0	0.99(2)	
Mg2	16*d*	$\frac{5}{8}$	$\frac{5}{8}$	$\frac{5}{8}$	0.82(2)	
Rh	32*e*	0.40478(2)	x	x	0.792(7)	
B	8*b*	$\frac{1}{2}$	$\frac{1}{2}$	$\frac{1}{2}$	1.0(2)	
Atom	B_{11} [b]	B_{22}	B_{33}	B_{12}	B_{13}	B_{23}
Mg1	0.89(3)	B_{11}	1.20(6)	0.18(4)	0	0
Mg2	0.82(4)	B_{11}	B_{11}	−0.07(4)	B_{12}	B_{12}
Rh	0.79(1)	B_{11}	B_{11}	0.025(6)	B_{12}	B_{12}

[a] $B_{eq} = \frac{1}{3}[a^{*2}a^2B_{11} + b^{*2}b^2B_{22} + c^{*2}c^2B_{33} + 2aba^*b^*(\cos\gamma)B_{12} + 2aca^*c^*(\cos\beta)B_{13} + 2bcb^*c^*(\cos\alpha)B_{23}]$; the displacement parameter of the boron atom was refined isotropically.

[b] Anisotropic displacement parameter is defined as $\exp[-\frac{1}{4}(a^{*2}h^2B_{11} + b^{*2}k^2B_{22} + c^{*2}l^2B_{33} + 2a^*b^*hkB_{12} + 2a^*c^*hlB_{13} + 2b^*c^*klB_{23})]$.

Table 3
Selected interatomic distances in Mg_8Rh_4B

Atoms	Distance (Å)	Atoms	Distance (Å)
Mg1–2Rh	2.7184(4)	Rh–1B	2.0073(3)
2Rh	2.989(2)	3Mg1	2.7184(4)
2Mg2	3.033(1)	3Mg2	2.7287(3)
4Mg1	3.1649(5)	3Mg1	2.989(2)
4Mg1	3.431(2)	3Rh	3.2779(4)
1Mg1	3.435(3)		
Mg2–2B	2.6350(4)	B–4Rh	2.0073(3)
6Rh	2.7287(3)	4Mg2	2.6350(4)
6Mg1	3.033(1)	6Mg1	3.659(2)
6Mg2	4.3027(1)		

atoms were assumed to occupy the octahedrally coordinated voids, formed by the Nb atoms. In Re_3Al_2B [22] compound boron atoms were suggested to completely substitute the rhenium atoms in 16*d* position. However, the positions of the boron atoms in the crystal structures $Nb_2NiB_{0.16}$ and Re_3Al_2B were not refined. In contrast to these compounds, in the phase Mg_8Rh_4B the boron atoms occupy the tetrahedrally coordinated voids at 8*b* ($\frac{1}{2},\frac{1}{2},\frac{1}{2}$). Mg_8Rh_4B is the first representative of a boron-filled Ti_2Ni structure, where the boron position is well refined using X-ray single crystal diffraction data. It should be noted that the η phase was not found in the Mg–Rh–(H, D) systems (E = O, C, N) [20,35]. Apparently, a compound with the Ti_2Ni structure can be found in Mg–Rh–E system, when the tetrahedrally coordinated voids are occupied by hydrogen (deuterium) [20]. Thereby the boron atoms occupy only one type of tetrahedral voids [$\square Rh_4$] around the 8*b* site; the hydrogen atoms occupy both the 8*b* and 32*e* sites—the centers of the [$\square Rh_4$] and [$\square(Mg1)_3Rh$] tetrahedra. In the hydride, a partial occupation of the octahedral cavities was found, whereas these cavities are empty in the crystal structure of Mg_8Rh_4B.

3.4. The Ti_2Ni structure type and its representatives

The Ti_2Ni-type structure and the related η subcarbides and suboxides have been discovered and extensively investigated a long time ago [11,36–40]. Generally the A_2M compounds, crystallizing in this structure type, were described as typical intermetallic phases since their components are restricted entirely to members of the transition metal series and their structures contain atomic sites of high coordination similar to those in σ-FeCr, and μ-Co_7Mo_6 [3]. For the A_2M phases the A component is dominated by the IVth group of transition metals—Ti and Hf [3,4,13,37,41]. The binary phases with Ti or Hf as the A component were obtained in the A–M systems, where M = Co, Ni, Fe, Mn, Rh, Ir, Pt and some other metals. There are a few examples of this structure type with metals of the third group: Sc_2Ir [42] and Sc_2Ru [43]. Regarding the M component, η phases are mainly observed with 3*d* transition metals —Fe, Ni, Co, Mn— and with platinum metals —Rh, Pd, Ru, Pt [6,12,13,37,43]. Not all transition metals can form this type of crystal structure. Even the behavior of chemically close elements such as Zr and Hf is completely different: there are no representatives of the Ti_2Ni structure type in the binary systems of Zr [3,11,13] in contrast with numerous η phases with Hf as the A component [3,6,13]. A few compounds with the η structure containing non-transition metals, such as $(Mg_{1.5}Ti_{0.5})Ni$ [44], $(Mg_{1.5}Al_{0.5})Ni$ [44], $(Mg_{1.5}Co_{0.5})Co$ [45], $(Mg_{1.5}Al_{0.5})Pt$ [46], are also known. In these structures the $A1$ atomic position (48*f*) is occupied by an alkaline-earth metal. Up to now there are no binary η phases known with the A or M sublattice formed by non-transition elements only.

The early discussions about the stability of the Ti_2Ni structure type were based on two main criteria:

(a) *Size criterion*: the average $r(A)/r(M)$ ratio should be close to 1.19 (this value corresponds to the metal atom radii taken from the compilation of Teatum E., K. Gschneidner and I. Waber) and the deviation from the

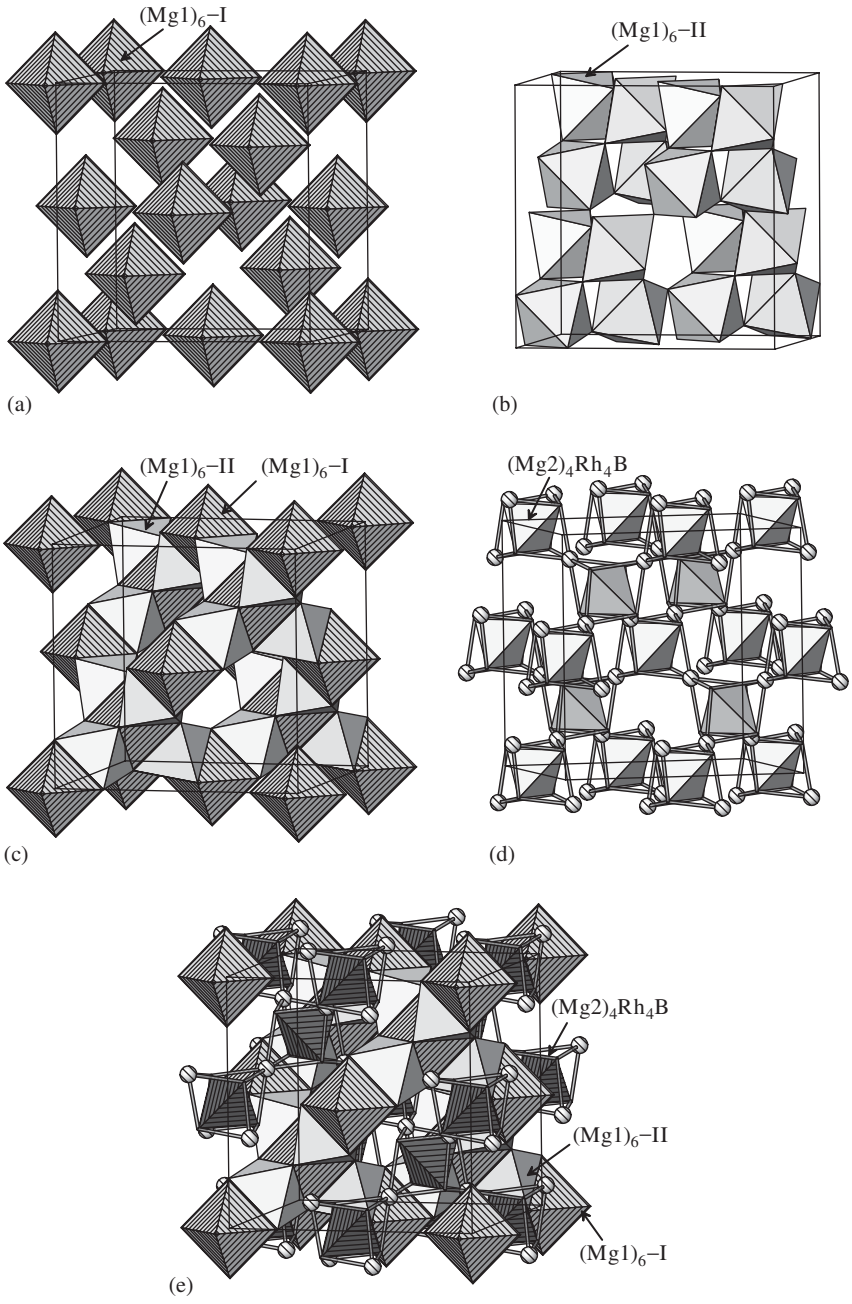

Fig. 3. Crystal structure of Mg_8Rh_4B: (a) isolated regular $(Mg1)_6$-I octahedra; (b) distorted $(Mg1)_6$-II octahedra connected by vertices; (c) framework formed by face-sharing $(Mg1)_6$-I and $(Mg1)_6$-II octahedra; (d) tetrahedral framework of *stellae quadrangula* $(Mg2)_4Rh_4B$; (e) interpenetration of the tetrahedral and two octahedral frameworks.

average should be smaller than 6% [3]. The size requirement is a necessary, but not a sufficient criterion. For example, it does not explain the absence of zirconium containing binary η phases Zr_2M ($R_{Zr}/R_M \approx 1.15-1.19$, where M belongs to the platinum group metals).

(b) *Criterion of the* "*electron concentration*:" i.e. the ratio of the number of valence electrons to the number of atoms, was formulated in [3,11,13] reflecting on the group number in the Periodic Table. A large number of η phases are formed by elements of the cobalt group [13]. The existence of ternary η phases with the M component consisting of two elements, one element lying to the right of the Co group in the Periodic Table and the second to the left of the Co group (for example $Hf_2Ni_{0.5}M_{0.5}$, M = Ru, Os, Re [3,13]), was considered as a confirmation of the "electron concentration" criterion, taking into account the absence of corresponding binary phases Hf_2Ni, Hf_2Os, Hf_2Ru, Hf_2Re, with the Ti_2Ni structure [3,13].

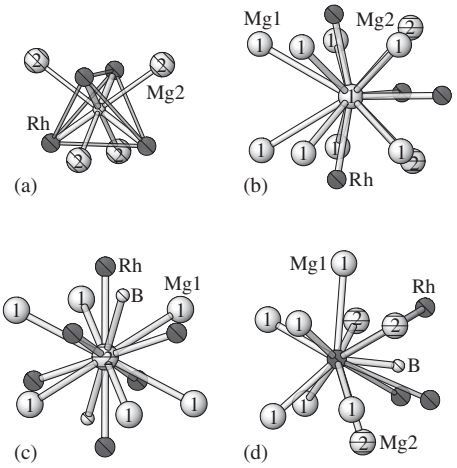

Fig. 4. Atomic environment in the crystal structure of Mg_8Rh_4B: B (a), Mg1 (b), Mg2 (c), Rh (d).

Any disscusion on the stability of the Ti_2Ni-type structure cannot be performed without considering the influence of an occupation of the interstitial sites. The unit cell of the Ti_2Ni structure contains 456 tetrahedral voids of six different types and 24 octahedral voids of two different types [7].

The incorporation of the elements $E = O$, N, C into the interstitial sites leads to the formation of ternary phases with the Ti_2NiE_x structure, which do not have binary analogues. Among the ternary η phases the most widely investigated classes are the ternary suboxides (e.g. Zr_2MO_x, $M = Ni$, Cu, Rh, Ir, Pt, V, Fe [10,12,13,17,47–49]) and subcarbides [18,19,36,40,50]. The structure refinement by neutron diffraction showed that oxygen and carbon atoms occupy the centers of the distorted $(A1)_6$-II octahedra (16*c* position) [2,10,14,17,47]. In spite of the existence of numerous binary and ternary compounds with the Ti_2Ni structure type, the chemical bonding in this structural motif and, consequently, the reasons for stabilization of the structure by incorporation of additional atoms are far from a complete understanding. A first attempt to explain qualitatively the oxygen influence on the structure stability was based on the analysis of electron donations to the conduction band, formed by the *M* atoms. Obviously, such donations lead to a partial ionization of the *M* species, so that the elements from groups with a lower number can provide more states [36], i.e. the *M*–O bonds are formed. In the Ti_2Ni structure the hybridizing *s* and *d* electrons of metals were suggested to be distributed between directed bonds and conduction band and there is a certain optimal electron/atom ratio for the structure formation. From this point of view, in the case of $M = Co$ and Ni, the number of electrons contributed to the conduction band leads to an optimal electron/atom ratio corresponding to the observed phase stability. If the *M* metal is an element, which provides more electrons, the increased filling of the conduction band destabilizes the structure. Oxygen, as an electron acceptor, decreases the number of occupied electronic states in the conduction band serving as an electron sink [36]. However, this explanation was only a suggestion and was not quantitatively confirmed.

Electronic structure calculations using extended Hückel method were first applied to understand the interstitial oxygen role as an electron acceptor and its effect on the metal–metal bonding for the zirconium–nickel suboxide Zr_4Ni_2O. The valence orbitals of the interstitial atoms were found to interact with the bonding orbitals of the transition metals. Thus, the balance between the strength of the metal–metal and metal–oxygen bonds was considered in the discussion on the stability of the Ti_2Ni structure type [17].

From the results above, the interplay between the directed (covalent) and non-directed (metallic) atomic interaction seems to play an important role for the stabilization of the Ti_2Ni structure motif. To get more insight into the directed interaction we performed an analysis of chemical bonding in Mg_8Rh_4B employing the ELF.

3.5. Chemical bonding in Mg_8Rh_4B

The topological description of the crystal structure of Mg_8Rh_4B as a filled variant of the Ti_2Ni structure type suggests a rather weak interaction of the implemented boron atoms with the metallic matrix. Despite this expectation, but in agreement with the fact that the binary Mg_8Rh_4 phase does not exist without boron, the calculation of the ELF reveals a strong covalent interaction within the $(Mg2)_4Rh_4B$ *stella quadrangula*. The maxima of ELF are located on the four Rh–B bonds (Fig. 5). The basins of these attractors form the valence shell of the boron atoms. Integration of the electron density inside this valence shell

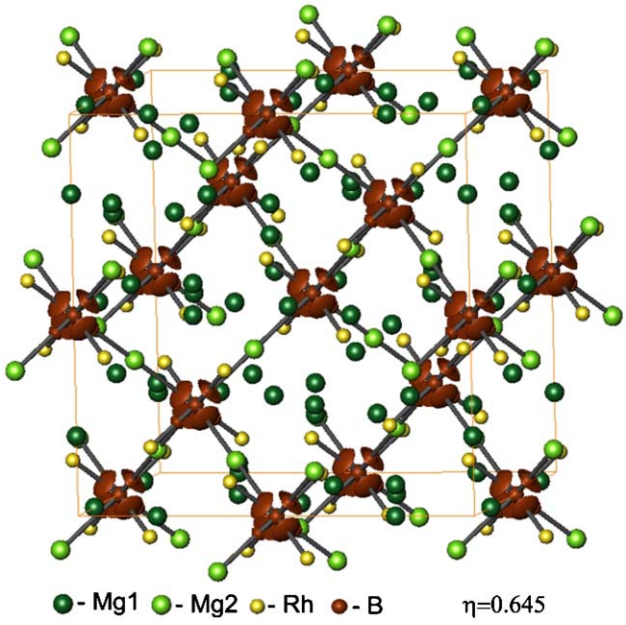

Fig. 5. Electron localization function for Mg_8Rh_4B: isosurfaces $\eta = 0.645$ revealing B–Rh bonds in the *stellae quadrangulae*.

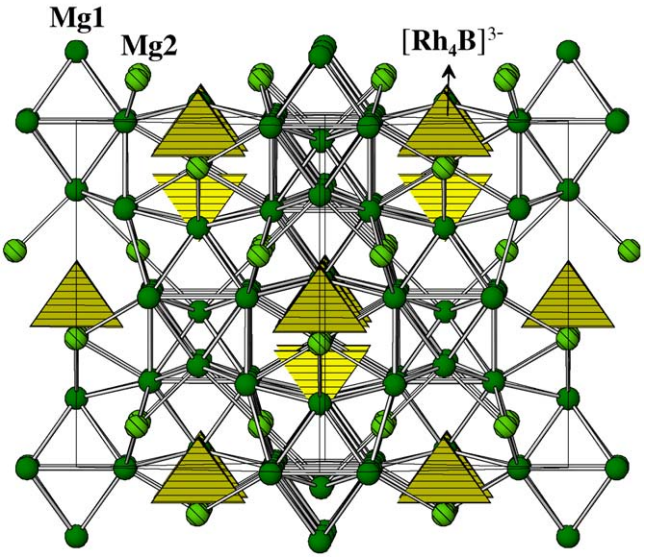

Fig. 6. Covalently bonded polyanions $[Rh_4B]^{3-}$ embedded in a cationic matrix in the crystal structure of Mg_8Rh_4B.

basin [51] results in 5.92 electrons. In the inner shells of the rhodium atoms, integration of the electron density gives $44.88 \approx 45$ electrons, in the inner shell of the boron atoms 2.1 electrons are found. In total this leads to a rhodium–boron anion $[Rh_4B]^{3-}$. The inner shells of the Mg2 atoms contain $10.03 \approx 10$ electrons each, thus revealing $(Mg2)^{2+}$ cations. A similar observation holds for the inner shells of the Mg1 atoms. From these findings, the total charge balance for Mg_8Rh_4B can be written as $[Mg^{2+}]_8[(Rh_4B)^{3-}] \cdot 13e^-$.

According to this bonding picture, the whole crystal structure, which by intuition could be rather metal-like, should be understood as composed of two parts: covalently bonded polyanions $[Rh_4B]^{3-}$ embedded in a cationic magnesium matrix (Fig. 6). The covalent interaction between Rh and boron in the polyanion $[Rh_4B]^{3-}$ and its ionic bonding within the cationic matrix is not so trivial, as it may looks like. On the one hand, this fact correlates with the practically equal electronegativities of Rh and B, both are much more electronegative as magnesium [33]. On the other hand, among the compounds in the ternary system Mg–Rh–B we observe different bonding depending on the composition. In the equiatomic compound $Mg_{1-x}RhB$ [52] rhodium and boron form together a 2D polyanion. An increase of magnesium and rhodium content in Mg_8Rh_4B does not change the covalent Rh–B interaction, but reduces the dimensionality of the anionic part ($[Rh_4B]^{3-}$ is an isolated entity). At the high boron content, in $Mg_2Rh_{1-x}B_{6+2x}$, rhodium, together with magnesium, acts as a cationic counterpart to a 3D boron polyanion [53]. The unusually large number of excess electrons suggests additional (covalent) interactions within the magnesium matrix. In the ELF representation, the directed (covalent) interaction is observed already in elemental metals in form of the multi-center bonding [54]. We assume a similar situation in the cationic matrix. For a more detailed proof of this assumption the ELF calculation should be done without an atomic sphere approximation. The development of a new tool for such calculations is in progress [55].

3.6. Magnetic and transport properties

The temperature dependence of the resistivity of the Mg_8Rh_4B sample is shown in Fig. 7a. Mg_8Rh_4B is quite a good metallic conductor with $\rho(300) - \rho_0$ ca. $90\,\mu\Omega\,cm$. The residual resistivity of the polycrystalline sample is $32\,\mu\Omega\,cm$. No phase transitions or superconductivity were detected.

The magnetic susceptibility $M(T)/H$ of a polycrystalline sample of Mg_8Rh_4B is displayed in Fig. 7b. The field dependence of M/H is due to traces of ferromagnetic impurities, which could not be detected by EDXS analysis. After the Honda–Owen extrapolation ([56], M/H vs. $1/H$ extrapolated to zero) the values of $\chi_{corr}(T)$ are obtained ($\chi_{corr}(300\,K) = +313(40) \times 10^{-6}\,emu\,mol^{-1}$). Mg_8Rh_4B is

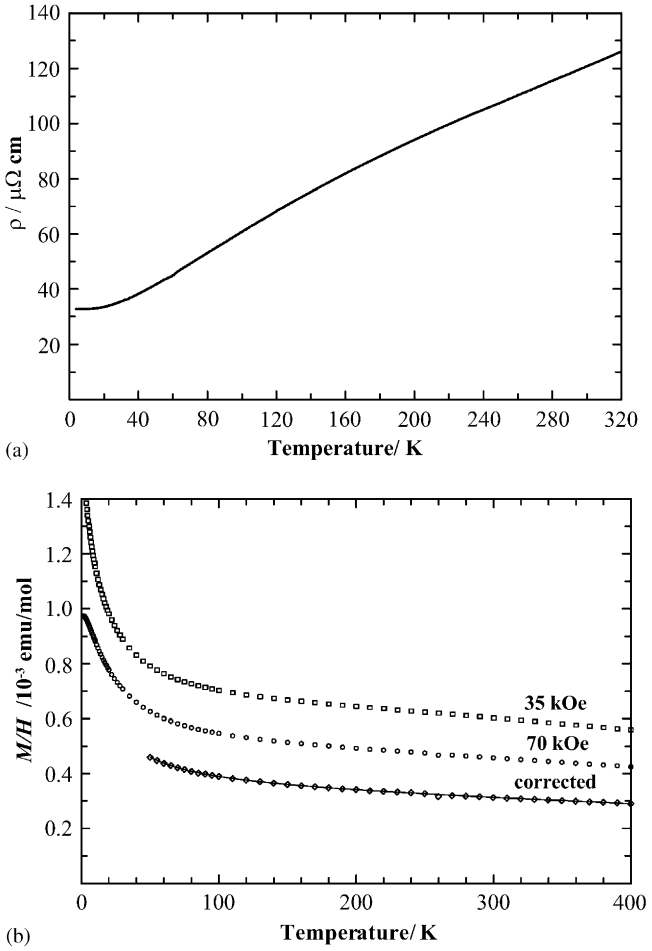

Fig. 7. (a) Resistivity ρ vs. temperature of a polycrystalline Mg_8Rh_4B sample. (b) Magnetic susceptibility χ of a polycrystalline Mg_8Rh_4B sample vs. temperature at magnetic fields $H = 35\,kOe$ (□), $70\,kOe$ (○), extrapolated values (◇) and modified Curie-fit.

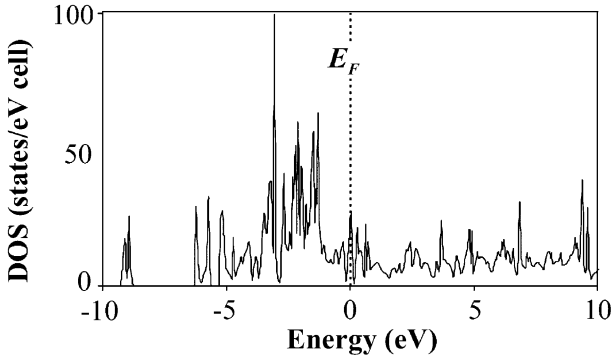

Fig. 8. Total electronic density of states for Mg_8R_4B.

therefore a Pauli paramagnet. Using the sum of the closed-shell diamagnetic increments ($\chi_{dia} = -96.2 \times 10^{-6}$ emu mol^{-1} [57]) and fitting the corrected susceptibility by a modified Curie law

$$\chi_{corr}(T) - \chi_{dia} = C/T + \chi_0 + \chi_1 T,$$

a value $\chi_0 = +440(40) \times 10^{-6}$ emu mol^{-1} is obtained. This corresponds to a density of states of 13.6 ± 1.2 states/eV per f.u. at the Fermi level.

The results of the electronic structure calculation are in agreement with the physical properties of Mg_8Rh_4B. The total density of states at the Fermi level is 9.25 states/eV per f.u. (Fig. 8), that is close to the value evaluated from magnetic measurements.

4. Conclusions

The Mg_8Rh_4B phase is the first representative of a boron-stabilized Ti_2Ni-type structure with filled tetrahedral holes. Analysis of the chemical bonding using the ELF shows that the structure stability is achieved by the formation of covalently bonded $[Rh_4B]^{3-}$ anions, embedded in a cationic magnesium matrix. The compound is a Pauli paramagnet and shows metal-like electrical conductivity, reflecting the picture of covalent bonding with excess electrons.

Acknowledgments

The authors thank Dr. Gudrun Auffermann and Mrs. Ulrike Schmidt for the chemical analyses; Mrs. Susann Müller for the DTA/DSC measurements. Dr. Ulrich Burkhardt is acknowledged for the metallographic preparation; Dr. Reiner Ramlau and Mrs. Katja Schulze are thanked for the EDXS measurements. A. M. Abakumov is grateful to the Russian Science Support Foundation for the financial support.

References

[1] J.K. Critchley, J.W. Jeffery, Acta Crystallogr. 19 (1965) 674.
[2] M.H. Mueller, H.W. Knott, Trans. Met. Soc. AIME 227 (1963) 674.
[3] M.V. Nevitt, Alloy Chemistry, in: P.A. Beck (Ed.), Electronic structure and alloy chemistry of the transition elements, New York, London, 1962, p. 127.
[4] S.N. Klyamkin, K.N. Semenenko, J. Alloys Compd. 293–295 (1999) 426.
[5] H.T. Takeshita, H. Tanaka, N. Kuriyama, T. Sakai, I. Uehara, M. Haruta, J. Alloys Compd. 311 (2000) 188.
[6] R.M. Van Essen, K.H.J. Buschow, J. Less-Common Met. 64 (1979) 277.
[7] A.L. Buzlukov, A.V. Skripov, A.V. Solonin, V.N. Kozhanov, A.P. Stepanov, J. Alloys Compd. 352 (2003) 66.
[8] A. Takasaki, V.T. Huett, K.F. Kelton, J. Non-Cryst. Solids 334 and 335 (2004) 457.
[9] J.S. Cantrell, R.C. Bowman Jr., A.J. Maeland, J. Alloys Compd. 330–332 (2002) 191.
[10] I. Yu. Zavaliy, W.B. Yelon, P.Y. Zavalij, I.V. Saldan, V.K. Pecharsky, J. Alloys Compd. 309 (2000) 75.
[11] M.V. Nevitt, L.H. Schwartz, Trans. Met. Soc. AIME October (1958) 700.
[12] I. Yu. Zavaliy, A.B. Riabov, V.A. Yartys, G. Wiesinger, H. Michor, G. Hilscher, J. Alloys Compd. 265 (1998) 6.
[13] M.V. Nevitt, J.W. Downey, R.A. Morris, Trans. Met. Soc. AIME 218 (1960) 1019.
[14] C. Stioui, D. Fruchart, A. Rouault, R. Fruchart, E. Roudant, J. Rebiere, Mater. Res. Bull. 16 (1981) 869.
[15] D.G. Westlake, J. Chem. Phys. 79 (9) (1983) 4532.
[16] D.G. Westlake, J. Less-Common Met. 105 (1985) 69.
[17] R. Mackay, G.J. Miller, H.F. Franzen, J. Alloys Compd. 204 (1994) 109.
[18] E. Parthe, W. Jeitschko, Acta Crystallogr. 19 (1965) 1031.
[19] K. Kuo, Acta Metall. 1 (1953) 301.
[20] F. Bonhomme, P. Selvam, M. Yoshida, K. Yvon, P. Fisher, J. Alloys Compd. 178 (1992) 167.
[21] A.S. Sobolev, Yu.B. Kuzma, T.F. Fedorov, Neorg. Mater. III (4) (1967) 638 (in Russian).
[22] N.F. Chaban, Yu.B. Kuzma, Neorg. Mater. VIII (6) (1972) 1065 (in Russian).
[23] W. Jeitschko, H. Holleck, H. Nowotny, F. Benesovsky, Monatsh. Chem. 95 (1964) 1004.
[24] M. Kolenda, A. Szytula, J. Leciejewicz, A. Pawlukojć, H. Ptasiewicz-Bak, J. Magn. Magn. Mater. 89 (1990) 26.
[25] L.G. Akselrud, P.Yu. Zavalii, Yu. Grin, V.K. Pecharsky, B. Baumgartner, E. Wölfel, Mater. Sci. Forum 335 (1993) 133.
[26] U. Burkhardt, Scientific Report MPI CPfS 2001/2002, Dresden January, 2003, p. 39.
[27] O. Jepsen, A. Burkhardt, O. K. Andersen, The Program TB-LMTO-ASA. Version 4.7. Max-Planck-Institut für Festkörperforschung, Stuttgart, 1999.
[28] U. Barth, L. Hedin, J. Phys. C 5 (1972) 1629.
[29] O.K. Andersen, Phys. Rev. B 12 (1975) 3060.
[30] A. Savin, H.J. Flad, H. Preuss, H.G. von Schnering, Angew. Chem. 104 (1992) 185;
A. Savin, H.J. Flad, H. Preuss, H.G. von Schnering, Angew. Chem. Int. Ed. Engl. 31 (1992) 185.
[31] M. Kohout, Basin. Version 2.3. Max-Planck-Institut für Chemische Physik fester Stoffe, Dresden, 2001.
[32] R.F.W. Bader, Atoms in molecules: a quantum theory, Oxford University Press, Oxford, 1999.
[33] J. Emsley, The elements, Oxford Chemistry Guides, London, 1991.
[34] B.G. Hyde, S. Andersson, Inorganic Crystal Structures, Wiley-Interscience Publication, New York, 1989.
[35] F. Bonhomme, K. Yvon, P. Fisher, J. Alloys Comp. 186 (1992) 209.
[36] M.V. Nevitt, Trans. Met. Soc. AIME 218 (1960) 327.
[37] W. Rostoker, Trans. AIME J. Metals February (1952) 209.
[38] N. Schönberg, Acta Metall. 3 (1955) 14.
[39] G.A. Yurko, J.W. Barton, J. Gordon Parr, Acta Crystallogr. 12 (1959) 909.
[40] N. Schönberg, Acta Chem. Scand. 8 (6) (1954) 932.

[41] A. Raman, K. Schubert, Z. Metallkde. 55 (11) (1964) 704.
[42] V.N. Yeremenko, V.G. Khorujaya, P.S. Martsenyuk, J. Alloys Compd. 204 (1994) 83.
[43] V.N. Eremenko, V.G. Khorujaya, P.S. Martsenyuk, K. Ye. Korniyenko, J. Aloys. Comp. 217 (1995) 213.
[44] L. Guanglie, Ch. Linchen, W. Lianbang, Y. Huantang, J. Alloys Compd. 321 (2001) L1.
[45] M. Yoshida, F. Bonhomme, K. Yvon, P. Fisher, J. Alloys Compd. 190 (1993) L45.
[46] K.J. Range, F. Rau, U. Klement, Acta Crysttallogr. C 46 (1990) 2454.
[47] F.J. Rotella, H.E. Flotow, D.M. Gruen, J.D. Jorgensen, J. Chem. Phys. 79 (9) (1983) 4522.
[48] A.B. Riabov, V.A. Yartys, B.C. Hauback, P.W. Guegan, G. Wiesinger, I.R. Harris, J. Alloys Compd. 293–295 (1999) 93.
[49] I. Yu. Zavaliy, M.V. Lototsky, A.B. Riabov, V.A. Yartys, J. Alloys Compd. 219 (1995) 38.
[50] W. Rostoker, Trans. AIME, J. Metals January (1955) 113.
[51] M. Kohout, F.R. Wagner, Yu. Grin, Theoret. Chem. Acc. 108 (2005) 150.
[52] A.M. Alekseeva, A.M. Abakumov, A. Leithe-Jasper, W. Schnelle, Yu. Prots, J. Hadermann, G. Van. Tendeloo, E.V. Antipov, Yu. Grin, Z. Anorg. Allg. Chem. 631 (2005) 1047.
[53] A.M. Alekseeva, A.M. Abakumov, A. Leithe-Jasper, W. Schnelle, Yu. Prots, E.V. Antipov, Yu. Grin, 9th European Conference on Solid State Chemistry, Stuttgart, 2003, p. 227.
[54] B. Silvi, C. Gatti, J. Phys. Chem. A 104 (2004) 947.
[55] A. Ormeci, H. Rosner, F. R. Wagner, M. Kohout, Yu. Grin, J. Phys. Chem. (2005), in press.
[56] K. Honda, Ann. Phys. 32 (1910) 1027.
[57] P.W. Selwood, Magnetochemistry, second ed, Interscience, New York, 1956.
[58] M. Sheldrick, SHELXS 97, Programs of Crystal Structure Analysis (Release 97-2), University of Göttingen, Germany, 1997.